Available online at www.sciencedirect.com
ScienceDirect
Optics Communications 274 (2007) 94–99
OPTICS COMMUNICATIONS
www.elsevier.com/locate/optcom

Beam profile characteristics of InGaAs sub-monolayer quantum-dot photonic-crystal VCSELs

Hung-Pin D. Yang [a,*], I-Chen Hsu [b], Fang-I Lai [b], Gray Lin [a], Ru-Shang Hsiao [a], Nikolai A. Maleev [c], Sergej A. Blokhin [c], Hao-Chung Kuo [b], Jim Y. Chi [a]

[a] *Nanophotonic Center, Industrial Technology Research Institute, Chutung 310, Hsinchu, Taiwan*
[b] *Institute of Electro-Optical Engineering, National Chiao Tung University, 1001 Ta Hsueh Road, Hsinchu 30050, Taiwan*
[c] *Ioffe Physico-Technical Institute, St. Petersburg 194021, Russia*

Received 24 April 2006; received in revised form 29 January 2007; accepted 29 January 2007

Abstract

An InGaAs sub-monolayer (SML) quantum dot photonic crystal vertical-cavity surface-emitting laser (QD PhC-VCSEL) for fiber-optic applications is first time demonstrated. The active region of the device contains 3 InGaAs SML QD layers. Each of the InGaAs SML QD layer is formed by alternate deposition of InAs (<1 ML) and GaAs. Single fundamental mode CW output power of 3.8 mW at 28 mA has been achieved in the 990 nm range, with a threshold current of 0.9 mA. Side-mode suppression ratio (SMSR) larger than 35 dB has been demonstrated over entire current operation range. The beam profile study of the PhC-VCSEL indicates that the laser beam is well confined by the photonic crystal structure of the device. The divergence angle of the devices remains almost unchanged with increasing current.
© 2007 Elsevier B.V. All rights reserved.

1. Introduction

Vertical-cavity surface-emitting lasers (VCSELs) have attracted a lot of attention in recent years. Single-mode VCSELs are necessary for a number of applications, including high-speed laser printing, optical storage and long-wavelength telecommunications. Small oxide aperture VCSELs below about 4 μm diameter operate in the fundamental transverse mode. However, the large resistance inherited from the small aperture limits the modulation bandwidth and degrades the high-speed performance. The lifetime of the oxide VCSEL also decreases proportionally to the diameter of the oxide aperture, even when the device is operated at a reduced current [1]. When the aperture diameter is increased to obtain higher output power, however, multiple higher-order transverse modes oscillate, causing increased noise, a broadened spectrum, and a strong increase of the far-field angle. Techniques used to solve the problem include the increase of higher order mode loss by surface-relief etching [2], hybrid oxide-implanted VCSELs [3,4] and two-dimensional triangular holey structure [5]. Recently, two-dimensional photonic crystal (2-D PhC) structure formed on the VCSEL surface has been used as a control method of transverse modes. Single-mode output was realized from larger aperture photonic crystal VCSELs (PhC-VCSELs) [6,7]. However, those PhC-VCSELs exhibit relatively high threshold currents (I_{th}) due to large oxide confined apertures. For long-wavelength applications, InAs quantum-dot (QD) VCSELs [8] and QD PhC-VCSELs [9] achieved laser emission at 1300 nm. For shorter wavelength emission, InGaAs/GaAs sub-monolayer (SML) quantum dot (QD), embedded in a GaAs matrix shows luminescence peaks and high power lasing performance in the 0.92–1 μm range [10].

Recently single-mode InGaAs SML QD VCSELs with room-temperature output power as high as 4 mW have

* Corresponding author. Tel.: +886 35915126; fax: +886 35915138.
E-mail address: hpyang@itri.org.tw (H.-P.D. Yang).

0030-4018/$ - see front matter © 2007 Elsevier B.V. All rights reserved.
doi:10.1016/j.optcom.2007.01.063

been demonstrated [11]. However single-mode operation of the InGaAs SML QD VCSEL with PhC is still yet to be realized. In this paper, we report our results on the InGaAs QD PhC-VCSELs in the 990 nm range. Single-transverse-mode operation with very high side-mode suppression ratio (SMSR) is demonstrated for the first time. The beam profiles of the PhC-VCSELs were measured and analyzed.

2. Epitaxial growth and device fabrication

The epitaxial layers of the InGaAs SML QD PhC-VCSEL wafers were grown on 3-in. n^+-GaAs(001) substrates by molecular beam epitaxy (MBE) in Riber 49 chamber. The bottom distributed Bragg reflector (DBR) consists of a 33-pair n-type (Si-doped) quarter-wave stack ($\lambda/4$) of $Al_{0.9}Ga_{0.1}As$/GaAs. The top DBR consists of 20-period p-type (carbon-doped) $Al_{0.9}Ga_{0.1}As$/GaAs quarter-wave stack. Above that, is a heavily doped p-type GaAs contact layer. The undoped 1λ-cavity contains 3 InGaAs SML QD layers, separated by GaAs barrier layers. Each of the InGaAs SML QD layer is formed by alternate deposition of InAs (<1 ML) and GaAs. A 200-nm-thick AlAs oxidation layer is placed within the p-type $Al_{0.9}Ga_{0.1}As$ confinement layer. Firstly, mesas with diameters varied from 50 to 68 μm was defined by reactive ion etch (RIE). The p-contact ring with an inner diameter 4 μm larger than the oxide aperture was formed on the top of p-contact layer. The AlAs layer within the $Al_{0.9}Ga_{0.1}As$ confinement layer was selectively oxidized to AlO_x. The oxidation depth was about 15–16 μm toward the center from the mesa edge so that the resulting oxide aperture varied from 18 to 38 μm in diameter. The oxide aperture was introduced in minimum of optical filed in order to reduce the lateral optical loss and the leakage current. The n-contact was formed at the bottom of the n^+-GaAs substrate. After that, triangular lattice patterns of photonic crystal with a single-point defect in the center were defined within the p-contact ring using photo-lithography and etched through the p-type DBR using RIE. The lateral index around a single defect can be controlled by the hole diameter (α)-to-lattice constant (Λ) ratio and etching depth [6]. This ratio (α/Λ) is 0.5; the lattice constant Λ is 5 μm in the PhC-VCSEL and the etching depth of the holes is about 16-pair thick into the 20-pair top DBR layer. The device structure is shown in Fig. 1. By using two types of apertures in this device, we decouple the effects of the current confinement from the optical confinement. The selectively oxidized AlO_x layer is used to confine the current flow, while the single-point defect (approximately $\geqslant 10$ μm in diameter) photonic crystal is used to confine the optical mode. In order to clarify the effect of photonic crystal index-guiding layer, an oxide-confined VCSEL (oxide aperture is approximately 18–20 μm in diameter without PhC) was also fabricated for comparison.

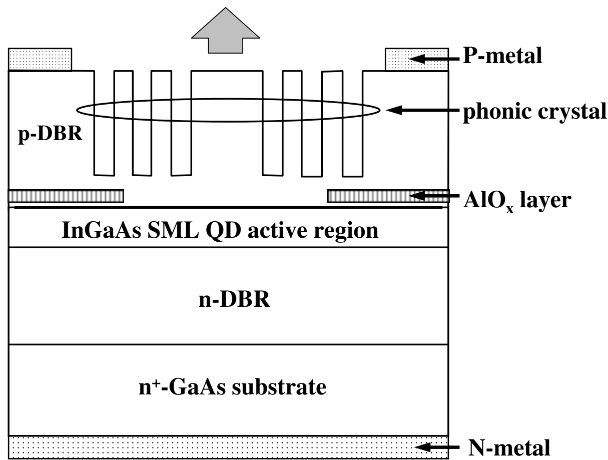

Fig. 1. Schematic of InGaAs SML QD PhC-VCSEL. The hole etching depth of the PhC is 16 pairs out of the 20-pair top DBR been etched off.

3. Results and discussions

The continuous-wave (CW) light–current–voltage (*L*–*I*–*V*) output of the InGaAs SML QD VCSEL without photonic crystal (PhC) is shown is Fig. 2a. The maximum output power is 12.2 mW at 30 mA, with a threshold current (I_{th}) of approximately 1–2 mA. The slope efficiency is 0.45–0.65 W/A from 1.5 to 16 mA. The device shows multiple transverse mode characteristics. The differential series resistance of the VCSEL without PhC is approximately

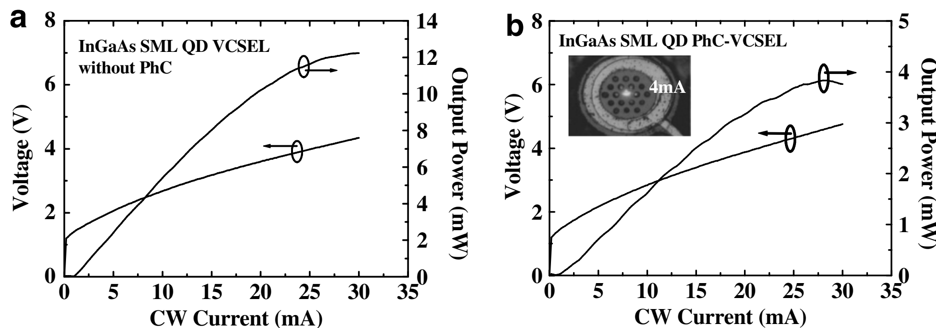

Fig. 2. CW *L*–*I*–*V* characteristics of the InGaAs SML QD (a) VCSEL without PhC and (b) PhC-VCSEL. The ratio α/Λ is 0.5 and the lattice constant Λ is 5 μm for the PhC-VCSEL. The near-field image of the PhC-VCSEL at 4 mA is shown in the inset.

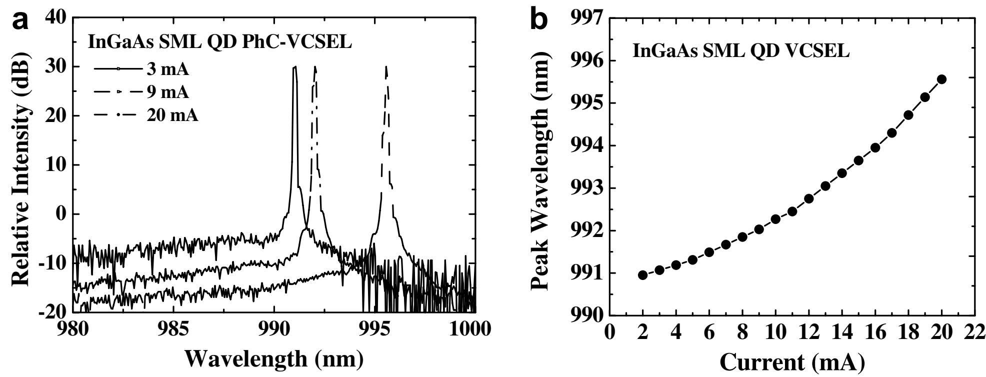

Fig. 3. (a) Spectra and (b) current-dependent peak wavelength of an InGaAs SML QD PhC-VCSEL.

100 Ω at 12 mA. The mesa of the VCSEL is 50 μm in diameter. Fig. 2b shows CW *L–I–V* output of the PhC-VCSEL. The near-field image of the PhC-VCSEL operated at 4 mA is also shown (inset). The I_{th} of the PhC-VCSEL is 0.9 mA, with an oxide aperture of approximately 18 μm in diameter. The PhC-VCSEL emits 3.8-mW maximum power at 28 mA and exhibits single mode operation throughout the current range of operation. This is one of the highest output power achieved for PhC-VCSELs. The slope efficiency is approximately 0.15–0.22 W/A from 3 to 15 mA. The slightly wiggly *L–I* current may be due to diffraction and optical scattering loss of the lasing output by the photonic crystal holes. The near-field image of the lasing output remains to be fundamental TEM_{00} mode at the center of the PhC structure throughout the current operating range. From the near-field image, laser emission from the six photonic crystal holes surrounding the single-point defect area was also observed. This laser emission from the photonic crystal holes corresponds to off-axis laser beam deviated from the optic axis perpendicular to the top-emitting surface of the VCSEL. The differential series resistance of the PhC-VCSEL is approximately 125 Ω at 12 mA. The *I–V* characteristics exhibit slightly higher series resistance for the PhC-VCSEL, which should be mainly due to blocking of the current flow in the region by photonic crystal holes. The *L–I* curve in Fig. 2b has lower slope efficiency than that of the 3 μm oxide aperture VCSEL of a previous work [11], which is mainly due to optical scattering loss by the photonic crystal holes. Higher order modes are suppressed by the photonic crystal structure of device. Current flows between the photonic crystal holes some may result in nonradiative recombination and spontaneous emission of

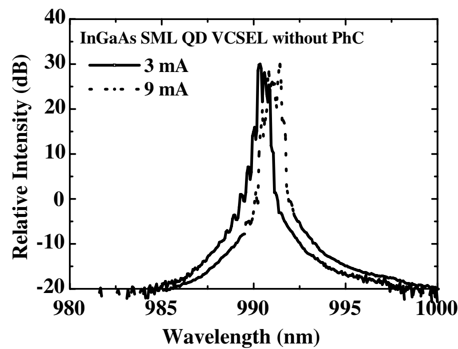

Fig. 4. Spectra of an InGaAs SML QD VCSEL without PhC.

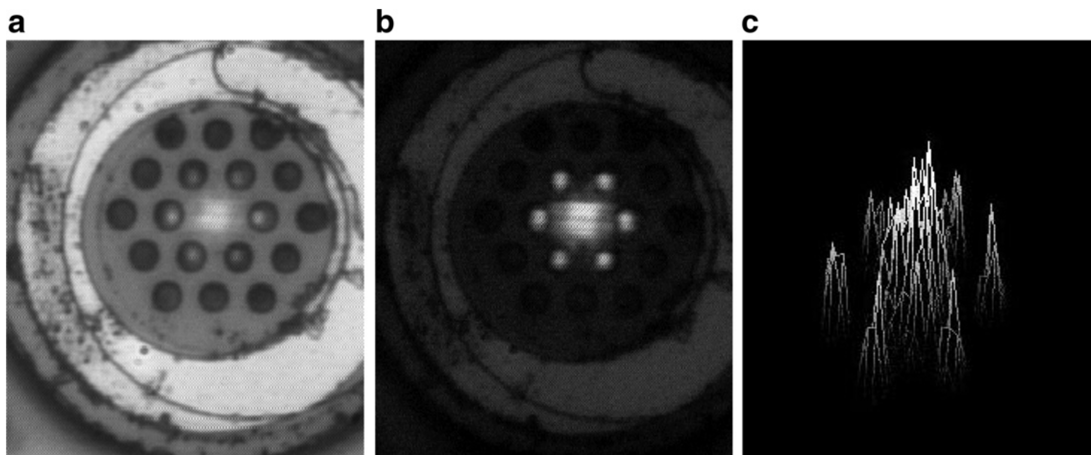

Fig. 5. (a) Photograph with biasing current at 10 mA, (b) near-field image at 14 mA, and (c) three-dimensional near-field intensity profile at 14 mA of the InGaAs SML QD PhC-VCSEL.

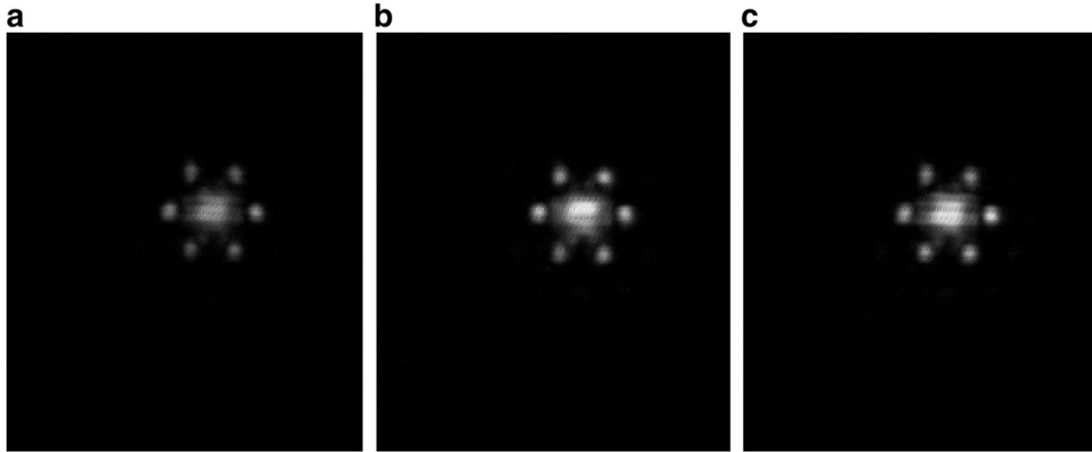

Fig. 6. Near-field images of InGaAs SML QD PhC-VCSEL at (a) 8 mA, (b) 16 mA, and (c) 20 mA.

Fig. 7. Near-field images of InGaAs SML QD VCSEL without PhC at (a) 3 mA, (b) 7 mA, and (c) 10 mA.

the injected carriers [12,13]. The formation of the phonic crystal holes is done by the RIE, which can also generate defects and surface states on the side-walls and etched surface of the etched holes. These defects and surface states can act as traps for the injected carriers [13]. However, the smaller series resistance of the PhC-VCSELs can delay the occurrence of thermal roll-over, which can therefore achieve higher output power.

Lasing spectra of the PhC-VCSEL is shown in Fig. 3a, confirming single-mode operation within overall operation current. The peak lasing wavelengths are 991, 992, and 996 nm at 3, 9, and 20 mA, respectively. The PhC-VCSEL exhibits a SMSR > 35 dB throughout the current range. Fig. 3b shows the current-dependent peak wavelength of the PhC-VCSEL. The peak lasing wavelength increases monotonically with the driving current.

For comparison, lasing spectra of the InGaAs SML QD VCSEL without photonic crystal holes shows multiple transverse mode operation as the driving current is increased above I_{th} (Fig. 4). The InGaAs SML QD VCSEL without PhC shows multiple transverse mode characteristics with a broader wavelength span. Fig. 5a is the photograph of the near-field image at 10 mA, with light illumination on the devices in order to show the laser emission pattern and the photonic crystal structure simultaneously. The fundamental TEM_{00} laser output is well confined at center of the single-point defect area. The near-field image at 14 mA is shown in Fig. 5b, and its three-dimensional near-field intensity profile shown in Fig. 5c. The laser beam emits not only from the single-point defect area at the center of the photonic crystal structure, but also from the six photonic crystal holes nearby. The three-dimensional near-field pattern analysis in Fig. 5c shows the laser output consists of one TEM_{00} mode emission at the center and six smaller beams with lower intensity. The laser beam intensity increases with increasing biasing current before thermal rollover occurs. The stray laser emission from the photonic crystal holes is believed

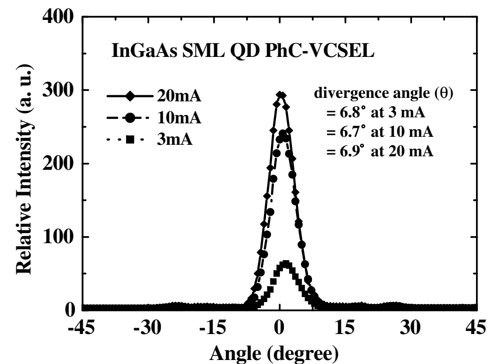

Fig. 8. Beam profiles of InGaAs SML QD PhC-VCSEL, measured at 3, 10, and 20 mA.

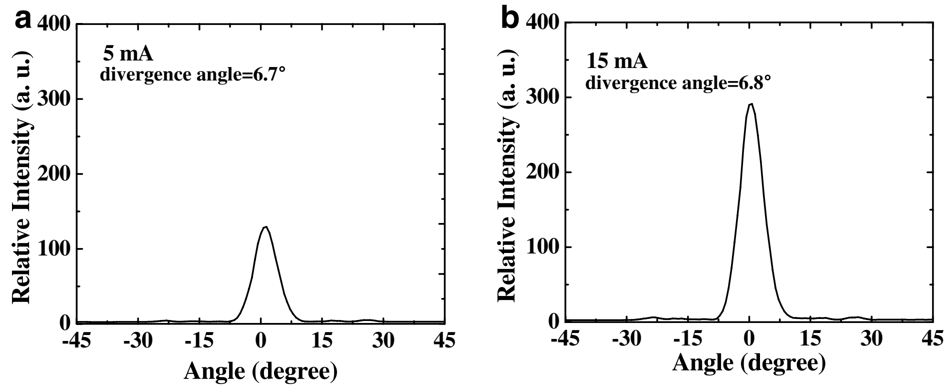

Fig. 9. Beam profiles of InGaAs SML QD PhC-VCSEL, measured at (a) 5 mA and (b) 15 mA.

to be the off-axis laser emission and diffraction within the laser cavity [14]. There is no other laser emission spot observed, indicating that there is no other lasing mode within the device. The laser beam that is not parallel to the optic axis of the laser cavity is referred to as the off-axis laser emission [14]. This off-axis laser emission also contributes to the divergence angle of the laser beam. The reflectance of the remaining p-DBR layers within the photonic crystal hole is significantly reduced due to RIE etch. The portion of the active region below the PhC hole cannot achieve lasing condition because of lower reflectance of the remaining p-type DBR layers. Therefore the laser emission from the photonic crystal holes must be contributed from off-axis laser emission and diffraction originated from the TEM_{00} mode at the center. Other stray laser emission was blocked by the high-reflectance top DBR. The measured single-mode spectra in Fig. 3 indicate that all the laser emission beams, including those from the photonic crystal holes, are of the same lasing wavelength. The spectral single-mode characteristics of the PhC-VCSEL are not affected by the laser emission from the photonic crystal holes. The calculated step in refractive index (Δn) is 4.2×10^{-3} for the photonic crystal structure with $\Lambda = 5$ μm and $\alpha/\Lambda = 0.5$. There is another effect for mode confinement, which is the refractive index difference ($\Delta n' \approx 2.4$) between air within the photonic crystal hole (refractive index = 1) and the semiconductor material of the VCSEL (refractive index ≈ 3.4). The cylindrical photonic crystal holes surrounding the single-point defect area can have certain confinement effect on the laser beam.

The near-field images of the PhC-VCSEL at 8, 16, and 20 mA are shown in Fig. 6. The stray laser emission from the six photonic crystal holes with smaller beam spot sizes was also observed at all current levels. The spot size of the fundamental TEM_{00} mode remains unchanged throughout the current range. The near-field images of the VCSEL without PhC at 3, 7, and 10 mA are shown in Fig. 7. The laser output exhibits multi-mode beam profile with higher intensity at the periphery. The laser output of the VCSEL without PhC is mainly confined by the AlO_x oxide aperture of the device. The intensity of the laser beam increases with increasing current.

The beam profile results obtained from the far-field beam divergence angle measurement system are shown in Figs. 8–11. The divergence angles are the full-width half-maximum (FWHM) of the measured beam profiles in Figs. 8–10. The beam profiles of the PhC-VCSEL are shown in Figs. 8 and 9. The beam divergence angle obtained from the beam profile of the device remains to be 6.7–6.9°. This very small divergence angle indicates that the laser beam is well confined by the photonic structure of the device. Fig. 10 shows the beam profiles of the VCSEL without PhC at 3, 7, and 10 mA. The divergence angle increases with increasing current, from 17.2° at 3 mA to 21.5° at 10 mA. The two laser emission lobes correspond to the annular-shaped laser emission observed by the near-field image in Fig. 7. Fig. 11 shows the current-dependent divergence angle of the InGaAs SML QD PhC-VCSEL and InGaAs SML QD VCSEL without PhC. For the InGaAs SML QD PhC-VCSEL, the divergence angle remains almost unchanged within 6.7–6.9°. For the InGaAs SML QD VCSEL without PhC, the divergence angle increases monotonically with current.

The polarization properties of the PhC-VCSELs were preliminarily studied. No significant polarization control by the photonic crystal structure was observed. The polarization direction of the PhC-VCSEL changes gradually with increasing current. The main reason is that the trian-

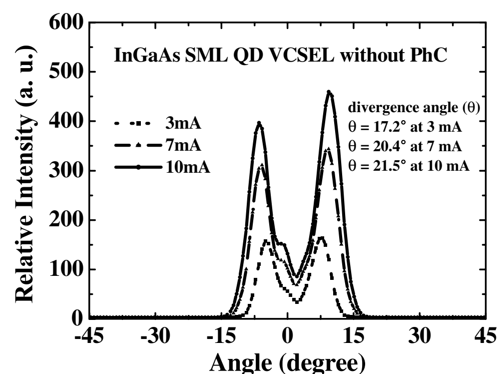

Fig. 10. Beam profiles of InGaAs SML QD VCSEL without PhC, measured at 3, 7, and 10 mA.

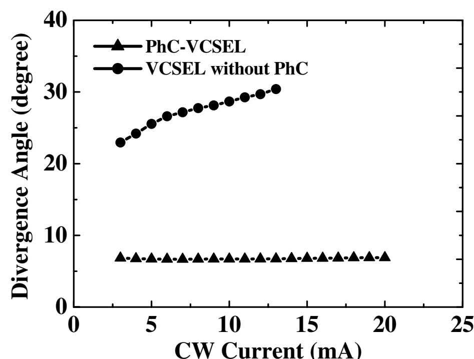

Fig. 11. Current-dependent beam divergence angle of the InGaAs SML QD PhC-VCSEL and InGaAs SML QD VCSEL without PhC.

gular lattice photonic crystal structure of the VCSEL is symmetrical geometrically, and so is the current injection profile. The controllable polarization switching of the VCSELs by asymmetrical current injection was studied by using a different device structure [15].

4. Conclusion

We report a single-mode InGaAs SML QD PhC-VCSEL with SMSR > 35 dB throughout the operation current range. A maximum single-mode output power of 3.8 mW has been demonstrated. The present results indicate that a VCSEL using an oxide layer for current confinement and photonic crystal for optical confinement is a promising approach to achieve single-mode operation of VCSEL. The beam profile study of the PhC-VCSEL indicates that the laser beam is well confined by the photonic crystal structure of the device.

Acknowledgements

The authors thank Dr. A.R. Kovsh of NL Nanosemiconductor GmbH in Germany for providing the InGaAs SML QD-VCSEL eptaxial wafers. This work was supported by the Nanophotonics Project, MOEA, Taiwan and SANDIA (NMP4-CT-2004-500101).

References

[1] B.M. Hawkins, R.A. Hawthorne III, J.K. Guenter, J.A. Tatum, J.R. Biard, in: 52nd Electronic Components and Technology Conference Proceedings, 2002, p. 540.
[2] A. Haglund, J.S. Gustavsson, J. Vukusic', P. Modh, A. Larsson, IEEE Photon. Technol. Lett. 16 (2004) 368.
[3] T.H. Hsueh, H.C. Kuo, F.I. Lai, L.H. Laih, S.C. Wang, Electron. Lett. 39 (2003) 1519.
[4] E.W. Young, K.D. Choquette, S.L. Chuang, K.M. Geib, A.J. Fischer, A.A. Allerman, IEEE Photon. Technol. Lett. 13 (2001) 927.
[5] A. Furukawa, S. Sasaki, M. Hoshi, A. Matsuzono, K. Moritoh, T. Baba, Appl. Phys. Lett. 85 (2004) 5161.
[6] N. Yokouchi, A.J. Danner, K.D. Choquette, Appl. Phys. Lett. 82 (2003) 1344.
[7] D. Berkedal, N. Gregersen, S. Bischoff, M. Madsen, F. Romsted, J. Oestergarrd, in: Optical Fiber Communication Conference Proceedings, 2003, p. 83.
[8] J.A. Lott, N.N. Ledentsov, V.M. Ustinov, N.A. Maleev, A.E. Zhukov, A.R. Kovsh, M.V. Maximov, B.V. Volvovik, Z.H.I. Alferov, D. Bimberg, Electron. Lett. 36 (2000) 1384.
[9] H.P.D. Yang, Y.H. Chang, F.I. Lai, H.C. Yu, Y.J. Hsu, G. Lin, R.S. Hsiao, H.C. Kuo, S.C. Wang, J.Y. Chi, Electron. Lett. 41 (2005) 1130.
[10] S.S. Mikhrin, A.E. Zhukov, A.R. Kovsh, N.A. Maleev, V.M. Ustinov, Yu.M. Shernyakov, I.P. Soshnikov, D.A. Livshits, I.S. Tarasov, D.A. Bedarev, B.V. Volovik, M.V. Maximov, A.F. Tsatsul'nikov, N.N. Ledentsov, P.S. Kop'ev, D. Bimberg, Z.H.I. Alferov, Semicond. Sci. Technol. 15 (2000) 1061.
[11] S.A. Blokhin, N.A. Maleev, A.G. Kuzmenkov, Yu.M. Shernyakov, I.I. Novikov, N. Yu. Gordeev, G.S. Sokolovskii, V.V. Dudelev, V.I. Kuchinskii, M.M. Kulagina, M.V. Maximov, V.M. Ustinov, A.R. Kovsh, S.S. Mikhrin, N.N. Ledentsov, Semiconductors 40 (2006) 663.
[12] G.P. Agrawal, N.K. Dutta, Semiconductor Lasers, second ed., Van Nostrand Reinhold, New York, NY, 1993 (Chapters 2 and 3).
[13] S.M. Sze, Physics of Semiconductor Devices, second ed., John Wiley and Sons, New York, NY, 1981 (Chapter 12).
[14] A.E. Siegman, Lasers, University Science Books, Mill Valley, CA, 1986 (Chapters 1 and 23).
[15] L.M. Augustin, E. Smalbrugge, K.D. Choquette, F. Karouta, R.C. Strijbos, G. Verschaffelt, E.–J. Geluk, T.G. van de Roer, H. Thienpont, IEEE Photon. Technol. Lett. 16 (3) (2004) 708.